

# Transport beam line for ultraslow monoenergetic antiprotons

K. Yoshiki Franzen<sup>a)</sup>

*Atomic Physics Laboratory, RIKEN, Wako 351-01, Japan*

N. Kuroda and H. A. Torii

*Institute of Physics, University of Tokyo, Komaba 3-8-1, Meguro-ku, Tokyo, Japan*

M. Hori

*CERN, CH-1211 Geneva 23, Switzerland*

Z. Wang, H. Higaki, and S. Yoneda

*Institute of Physics, University of Tokyo, Komaba 3-8-1, Meguro-ku, Tokyo, Japan*

B. Juhász

*Institute of Nuclear Research of the Hungarian Academy of Sciences, H-4001 Debrecen, Hungary*

D. Horváth

*KFKI Research Institute for Particle and Nuclear Physics, H-1525 Budapest, Hungary*

A. Mohri

*Atomic Physics Laboratory, RIKEN, Wako 351-01, Japan*

K. Komaki

*Institute of Physics, University of Tokyo, Komaba 3-8-1, Meguro-ku, Tokyo, Japan*

Y. Yamazaki<sup>b)</sup>

*Atomic Physics Laboratory, RIKEN, Wako 351-01, Japan*

(Received 9 January 2003; accepted 26 March 2003)

A beam line for the transportation of slow antiprotons from a multiring electrode trap to an experimental chamber is described. The beam line is equipped with a three-stage differential pumping system in order to maintain a pressure lower than  $1 \times 10^{-12}$  Torr in the trap region while simultaneously having a pressure of around  $1 \times 10^{-6}$  Torr in the chamber. Tests have shown that  $10^5$  positive ions per trapping cycle were successfully extracted at 250 eV from the trap positioned in a superconducting solenoid. The ions were then further transported through three small apertures to the target area located 3.5 m downstream of the trap. Results from the first delivery of a 250 eV antiproton beam are described. © 2003 American Institute of Physics. [DOI: 10.1063/1.1578160]

## I. INTRODUCTION

The recent advent of the Antiproton Decelerator (AD) at CERN has dramatically opened up new experimental opportunities to study the properties of the antiproton itself and its interaction with matter and antimatter at ultralow velocities, which includes antiprotonic atom formation processes under single collision conditions and high precision spectroscopy of metastable antiprotonic atoms, such as protonium, antihydrogen formation and its high precision spectroscopy, ionization processes of atomic hydrogen, etc.<sup>1</sup> An essential condition for the success of such experiments is the availability of a high-quality antiproton beam at very low energies. Previously, it was demonstrated that a 1–100 keV beam is obtained by passing the 5 MeV beam delivered by the AD through the Radio Frequency Quadrupole Decelerator (RFQD).<sup>2,3</sup> In order to reach even lower beam energies and thus further extend the experimental possibilities, the Atomic Spectroscopy and Collisions Using Slow Antiprotons

(ASACUSA) collaboration<sup>1</sup> has combined the RFQD with a large volume multiring trap (MRT) followed by a specially designed extraction beam line.<sup>4–7</sup> The MRT<sup>8</sup> traps, cools and then ejects a large number of cold antiprotons as a pulsed or continuous beam enabling interaction studies between antiprotons and matter in the hitherto unexplored energy region 10 to 1000 eV. As the first experiment, the formation processes of antiprotonic atoms under single collision conditions will be studied with the slow antiproton beam intersecting a gas jet of H<sub>2</sub> or noble gases. The target density should of course be as high as possible but since microchannel plate (MCP) detectors will be used in the target chamber the background pressure should not exceed  $1 \times 10^{-6}$  Torr. On the other hand, the pressure in the trap should be lower than  $1 \times 10^{-12}$  Torr because the survival lifetime of the antiprotons against annihilation with the residual gas should be longer than the time necessary for cooling and manipulation of antiprotons in the MRT, which is typically several tens of seconds. The trap must therefore be isolated from the target chamber by an extraction beam line equipped with several effective differential pumping stages. At the same time, the most important requirement is that the transport efficiency should be very high so that the precious slow antiprotons can

<sup>a)</sup>Electronic mail: franzen@phys.ufl.edu

<sup>b)</sup>Also at: Institute of Physics, University of Tokyo, Komaba 3-8-1, Meguro-ku, Tokyo, Japan.

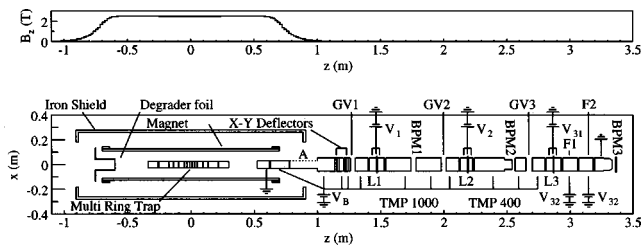


FIG. 1. Schematic view of the 5 T superconducting magnet, the trap electrodes, and the extraction beam line electrodes. The calculated magnetic field distributions  $B_z$  is also exhibited for a coil current corresponding to 2.5 T at the center of the magnet. GV: gatevalve, BPM: beam profile monitor, L: lens, V: voltage, TMP: turbo molecular pump, A: mesh, and F: electrode.

be used without loss. This article reports (1) the design procedure of the extraction beam line, which is specially prepared to fulfill the somewhat contradictory requirements just described, i.e., high transport efficiency and large differential pumping capability and (2) the result of test experiments with ions ( $p$ ,  $H_2^+$  and  $H_3^+$ ) and with ultraslow antiprotons for the first time.

## II. DESIGN

### A. Brief description of the trap

In order to describe how the beam line was designed, an outline of the antiproton trap is briefly described here. A more detailed report will be published elsewhere. The MRT<sup>8</sup> was adopted for the trapping and cooling of antiprotons because of its large catching volume and higher stability, which are necessary to handle a large number of charged particles while keeping the space-charge effects relatively small. The MRT was positioned at the center of the bore tube of a 5 T superconducting solenoid magnet as shown in Fig. 1. The design details of the solenoid and the MRT were reported previously.<sup>4,6</sup> The size of the solenoid is approximately 1.8 m in length and 22 cm in inner diameter. The inner diameter of the bore tube is 165 mm. Both ends of the bore tube are supported by eight motor controlled linear feedthrough rods (four rods on each side), which enables the precise alignment of the bore tube axis with respect to the solenoid axis. Charged particles were confined radially by a strong magnetic field and axially by electric fields produced by applying potentials to several ring electrodes of the MRT. It was demonstrated that our system was capable of trapping and confining more than  $10^6$  antiprotons per shot delivered from the AD together with approximately  $10^8$  preloaded electrons. The trapped antiprotons were sympathetically cooled via interactions with the electrons, which in turn cooled themselves by emitting synchrotron radiation in the strong magnetic field.<sup>9</sup> Details of this procedure are published elsewhere.<sup>10,11</sup> When the electrons needed to be removed from the MRT before antiproton extraction, either (1) the trapping potential was turned off for a short time (around 0.5  $\mu$ s) so that the electrons could escape while the slower antiprotons remain in the trap region or (2) a weak rf field with a frequency in resonance with the axial oscillations of the electron plasma was applied to one of the MRT electrodes for a fraction of a second. A dc extraction of antiprotons was

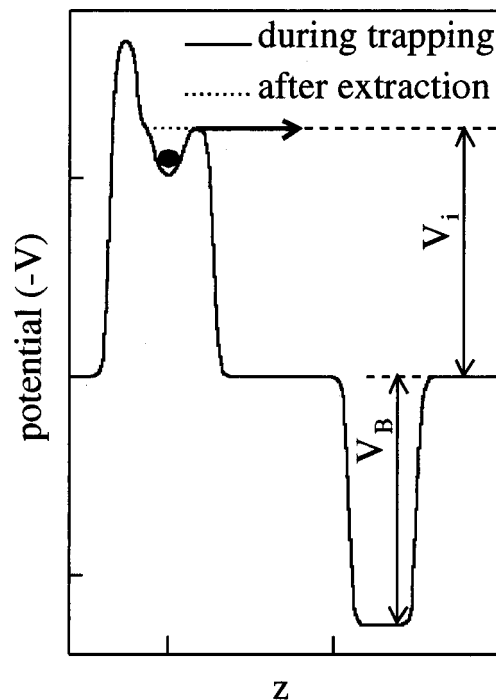


FIG. 2. Scheme of antiproton extraction from the trap region.

performed by slowly varying the trap depth while still keeping the barrier height at  $V_i$  as shown in Fig. 2. In this way, antiprotons in the MRT were flowing out continuously and a quasi-monoenergetic beam with a kinetic energy of  $eV_i$  was produced.

The pressure measured outside the bore tube was typically  $1 \times 10^{-10}$  Torr. Since the temperature of the bore tube was kept below 10 K during measurements, the pressure in the MRT region is expected to be at least one order of magnitude better than the aforementioned value. Two mylar degrader foils with a total thickness of 1.8  $\mu$ m were positioned 60 cm upstream of the center of the magnet. The antiproton beam delivered from the RFQD at around 100 keV was then decelerated down to less than 10 keV when traversing the foils. The foils also physically isolate the bore tube area from the RFQD area where the pressure is higher than  $1 \times 10^{-9}$  Torr.

### B. Requirements

The basic requirement of the extraction beam line are as follows: (1) to transport the cooled antiprotons from the MRT to the target area with a minimum of loss, (2) to focus the beam at the target with a minimum spot size, (3) to enable differential pumping with a pressure difference of more than six orders of magnitudes between the trap area and the target area, (4) to provide a variable beam energy at the target from 10 eV to 1000 eV, and (5) to be able to deliver the antiprotons both as a dc beam and as a pulsed beam of a few microseconds duration. The required pressure difference could only be realized with a series of differential pumping stages consisting of small apertures combined with an effective evacuation system.

Additional requirements were to prepare gaps of several centimeters between the cylindrical electrodes along the beam line so that two beam profile monitors (BPMs), three gate valves, and two pumping ports can be inserted. The gaps also help to effectively evacuate the volume surrounded by the electrodes. The system should also be able to inject electrons into the MRT for antiproton cooling. Furthermore, a set of  $x$  and  $y$  deflectors is necessary so that any misalignment between the trap and the beam line can be corrected.

**C. Simulations**

A difficulty arises when extracting charged particles from a strong magnetic field since the trajectories tend to follow the magnetic field lines, which are strongly diverging. Furthermore, when leaving the magnetic field the extracted particles increase their angular momentum, which limits later focusing of the beam. The situation was thus complicated and it was necessary to perform numerical simulations during the design of the beam line in order to optimize the transmission and quality of the beam. These calculations were performed with a commercial software (TriComp package, Field Precision Inc.), which utilizes a finite-element method to calculate the cylindrically symmetric fields from a given current and electric potential distributions taking into account the realistic susceptibility of the iron shield around the magnet (see Fig. 1). The calculated  $B_z$  distribution from a current corresponding to 2.5 T along the axis is drawn in the upper part of Fig. 1.

Trajectory calculations were performed for antiprotons starting from the trap region under influences of both magnetostatic and electrostatic forces. The accuracy of the calculations was examined by comparing the initial and final kinetic energies and total angular momenta. By performing the calculations with a field element size of around  $0.5 \text{ mm}^2$  and an orbit integration time step of around  $10^{-10} \text{ s}$ , trajectories with errors less than 1% were obtained. No further improvements in accuracy could be obtained by further reducing the element size or the orbit integration time step due to the accumulation of round off errors. It should be emphasized that the software uses a sophisticated method to interpolate the fields at the position of the moving particle from the vertices defining the element containing the particle at each step of the progressing trajectory.

In these calculations, it was assumed that the antiproton cloud in the trap is of a cylindrical shape 2 mm in diameter and with homogenous density. Furthermore, it was assumed that the antiprotons had energies of 1 eV in the perpendicular direction relative to the magnetic field. These assumptions were based on experiences from similar experiments.

An optimized ion optics configuration was thus obtained by a trial and error procedure. The final result is drawn in Fig. 1, which consists of two sets of  $x$  and  $y$  deflectors, two Einzel lenses (L1 and L2), and an asymmetric lens (L3). Five gaps for three gate valves (GV1, GV2, and GV3) and two beam profile monitors (BPM1 and BPM2) were also prepared to fulfill the requirements. The optimized spot size and the effective divergence at the end focal point are given in Table I for antiprotons of 10, 100, and 250 eV extracted from

TABLE I. Antiproton beam focal point parameters from simulations versus extraction energy. (See the text for the assumed parameters.)

Extraction energy $E$ (eV)	Effective beam radius $2x_{\text{rms}}$ (mm)	Effective divergence angle $2x'_{\text{rms}}$ (degrees)	$E^{-1/2} * 2x_{\text{rms}} * 2x'_{\text{rms}}$
10	3.1	$\pm 17.8$	175
100	2.5	$\pm 6.5$	162
250	2.2	$\pm 4.9$	170

the MRT with a magnetic field of 1 T. The effective values of the radius were defined by  $2x_{\text{rms}}$ , where  $x_{\text{rms}}$  is given by the root-mean square of one transversal coordinate at the focal point for all the trajectories studied. The effective values of the divergence angles were defined by  $2x'_{\text{rms}}$  where  $x'_{\text{rms}}$  is given by the root-mean square of the slopes relative to the beam line axis at the focal point for the same trajectories (see, e.g., Ref. 12). The right-hand side-most column of Table I shows a product of the square root of the projectile energy, the spot size, and the divergence angle, which is proportional to the normalized emittance. It is seen that the normalized emittance does not strongly depend on the final energy. The necessary potential configuration to get the optimized beam is shown in Fig. 3 as a function of the final energy of the antiprotons. It is noted that the initial transverse energy of 1 eV has only a minor effect on the final beam parameters, but that the initial radial distribution of the antiproton cloud plays the dominant role. This can be understood by comparing the magnetic and thermal components of the canonical angular momentum  $p_\theta$  of the antiprotons.<sup>13</sup> The magnetic component is given by  $eA_\theta r$  where  $r$  is the radial coordinate in a cylindrical coordinate system and  $A_\theta$  is the theta component of the vector potential which for a uniform field in the  $z$  direction is given by  $Br/2$  where  $B$  is the magnetic field in the trap. The thermal component is given by  $mv_\theta r$  where  $m$  is the antiproton mass and  $v_\theta$  is the theta

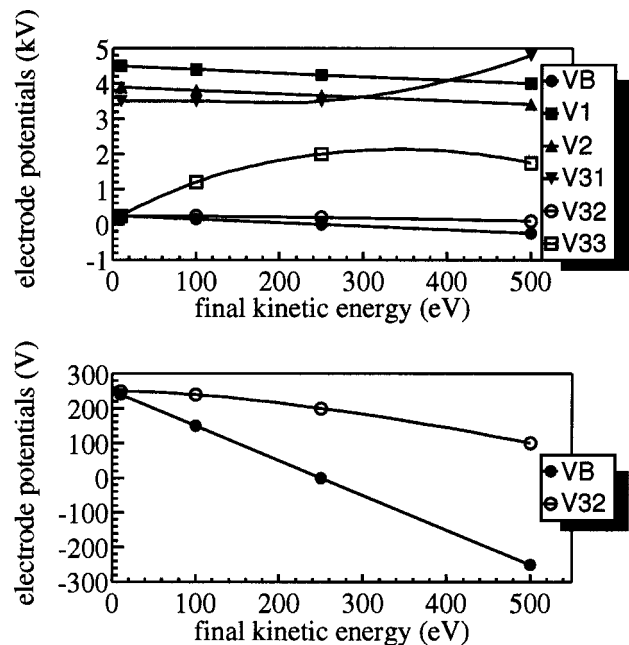


FIG. 3. Optimum electrode potentials as functions of extraction energy.

component of the transversal velocity. For example, the magnetic component of the canonical angular momentum of an antiproton at  $r=1$  mm and at 1 T is  $\sim 3.5$  times larger than the thermal component with a transverse kinetic energy of 1 eV. In other words, the key parameter to govern the emittance of the antiproton beam is not the temperature of the cloud but the radius and the field strength in the present conditions.

#### D. Transport scheme and design details

The barrier height of the downstream side of the MRT potential is set at  $V_i$ , which defines the final energy of antiprotons to be  $eV_i$  at the target point (see Fig. 2). After leaving the trap, the antiprotons travel with the same energy along the homogenous magnetic field, and then enter the beam line electrodes, where they are accelerated or decelerated to  $e(V_B + V_i)$ , which was around 250 eV (see Fig. 1). The beam then enters the first Einzel lens L1 biased at  $V_1$ . An Einzel lens usually consists of three metal tubes of the same diameter positioned coaxially after each other. Applying a decelerating or an accelerating potential to the middle electrode achieves focusing of a charged particle beam passing through the tubes. At a certain applied potential, an approaching parallel beam can be forced to have a radial node in the center of the middle electrode. This is true for both the deceleration mode and the acceleration mode. For the deceleration mode, the applied voltage would be close to stopping the incoming beam, while for the acceleration mode the applied voltage would increase the kinetic energy of the incoming beam many times while passing the center of the lens. Both of these operation modes are nonstandard in ion optics. In our case, a metal aperture was prepared at the center of the middle electrode for differential pumping. The aperture is biased to the same potential  $V_1$  as the middle electrode. It is noted that the aberration of the acceleration mode is much smaller than the deceleration mode. After being focused when entering L1 and passing the aperture, the beam is made parallel again to the beam line by being decelerated when again entering electrodes of potential  $V_B$  (see Fig. 1), and then proceeds to L2 and L3. The beam is finally focused on the target position (shown as BPM3 in Fig. 1) with the F1 and F2 electrodes of L3 biased at  $V_{32}$  and  $V_{33}$ . Examples of the beam envelope for the beam energies of 250 eV, 100 eV, and 10 eV are shown in Fig. 4 together with the respective electric potential distributions along the beam line axis. Electrons from a Spindt-type electron emitter were preinjected into the trap through a slot of 125 mm  $\times$  25 mm machined on electrode A as indicated in Fig. 1. The slot is covered with gold-plated tungsten wires with a 10  $\mu$ m diameter and a spacing 0.5 mm in order to allow electrons being injected from outside of the electrode but at the same time keeping the potential inside the electrode undisturbed. The position of the electron emitter was carefully determined employing trajectory simulations so that electrons from the emitter are guided into the trap by the magnetic field. The electrodes were made of aluminum, which was chosen since it is non-magnetic and a so-called ethanol lathing was applied. A thin and uniform layer of aluminum oxide is formed with this

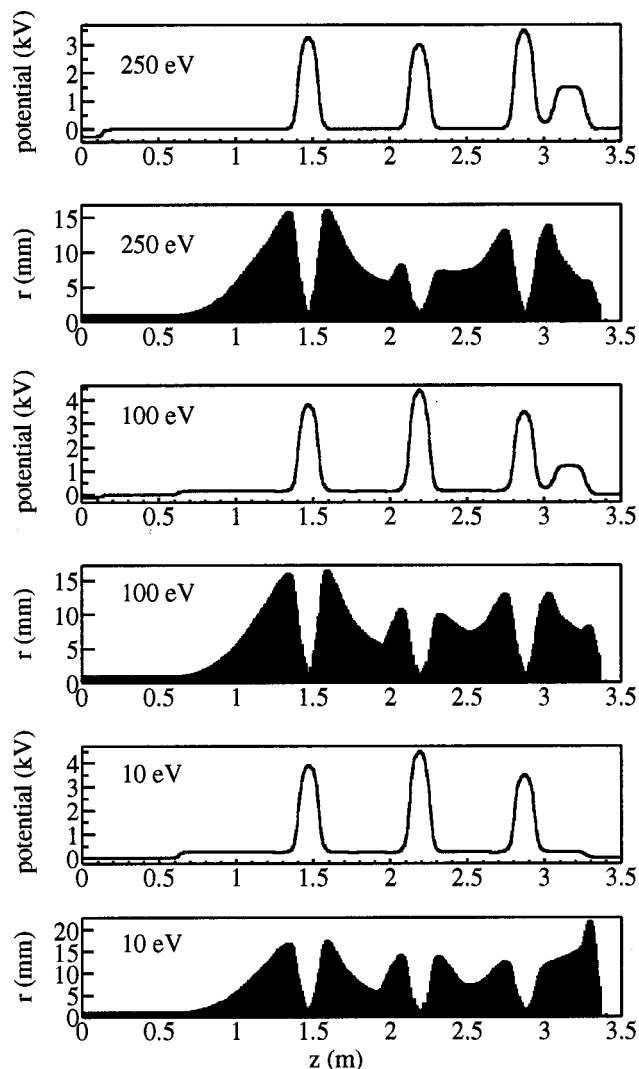


FIG. 4. Envelopes of antiproton trajectories traveling from the left- to the right-hand side through the electrodes of the extraction beam line for extraction energies of 250, 100, and 10 eV. The electric potential along the center axis is exhibited in the panels above each set of trajectories.

technique, which considerably reduces outgassing during evacuation. The potential to each electrode is supplied via CuBe springs touching the surface connecting to high-voltage electrical feedthroughs.

The extraction beam line is equipped with two BPMs. BPM1 is a RoentDek DL40 delay line anode MCP, which can detect ions of both polarities one by one with a position resolution of 0.1 mm and a time resolution of 500 ps. BPM1 was mounted on a linear translator, and could be removed from the beam line. BPM2 shown in Fig. 1 is a wire chamber detector,<sup>14</sup> which offers nondestructive monitoring of the beam in the case of a pulsed beam. During the test described later in this article, BPM3 (a second RoentDek detector) was positioned at the focal point of the beam line in order to measure the number and position of transmitted particles. BPM3 was movable along the beam axis in order to measure the emittance around the focal point.

As an aperture of 4 mm in diameter and a pump with an evacuation speed of 100 l/s provides a pressure difference of a factor of 100, three apertures with diameters variable from

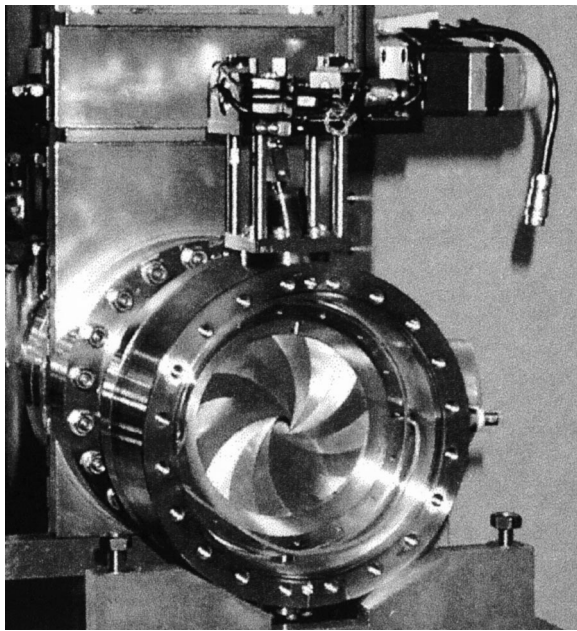


FIG. 5. A photo of the adjustable high-voltage aperture.

10 mm down to 4 mm were installed in the extraction beam line. A photo of such a high-voltage variable aperture is shown in Fig. 5. The extraction beam line was evacuated with turbomolecular pumps of evacuation speeds 1000 l/s and 400 l/s positioned as shown in Fig. 1. The base pressures were a few times  $10^{-10}$  Torr in the area between the two apertures of lenses L1 and L2, in the  $10^{-9}$  Torr range in the area between the two apertures of L2 and L3, and in the  $10^{-8}$  Torr range downstream of the aperture of L3. The differential pumping ability was tested by introducing He at a pressure of  $1 \times 10^{-6}$  Torr into a chamber connected to the end of the beam line. The chamber was pumped with a turbomolecular pump giving a background pressure of  $3 \times 10^{-8}$  Torr. With all three apertures set at a 4 mm diameter, the pressure measured between lenses L3 and L2 was approximately  $1 \times 10^{-7}$  Torr, between lenses L2 and L1 approximately  $1 \times 10^{-9}$  Torr, and at the downstream exit of the magnet bore tube approximately  $1 \times 10^{-10}$  Torr. It was therefore concluded that the efficiency meets the requirement and that some experiments might be performed with even bigger apertures than initially expected.

### III. EXPERIMENT

#### A. Protons, $H_2^+$ , and $H_3^+$ ions

As the first test of the beam line, positive ions were stored in the MRT by ionizing the residual gas with electrons of several hundred eV, and were then extracted and transported to the target position. In order to increase the ion production rate, the bore tube temperature was raised to around 100 K thus increasing the residual gas pressure. Since the main component of the residual gas was  $H_2$ , it is expected that the ions were mostly  $H_3^+$  and  $H^+$ ,<sup>11</sup> where the first component is formed through ion-molecule reactions like  $H_2^+ + H_2 \rightarrow H_3^+ + H$ . Before extraction through the beam line, the trap was biased to the required potential as de-

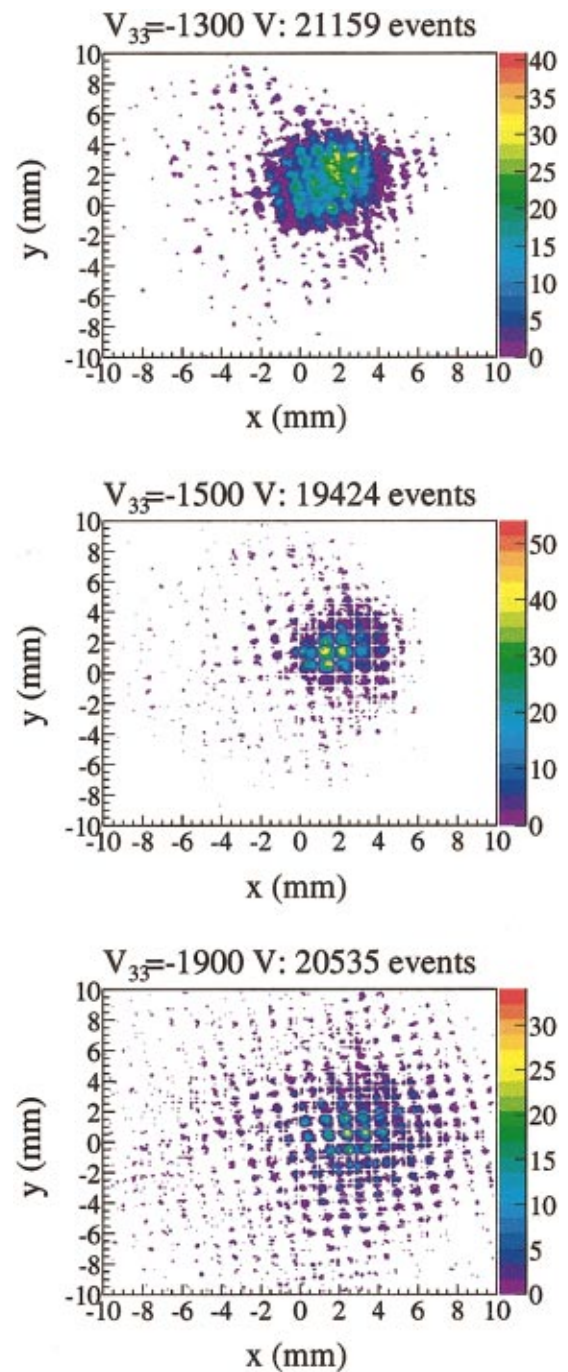


FIG. 6. (Color) Beam profile of 250 eV positive particles detected at the focal point of the beam line with a delay line anode MCP system for different focus conditions.

scribed earlier. A test of the pulsed extraction mode showed that an ion pulse of  $\sim 10^{-14}$  C ( $\sim 10^5$  ions) was extracted and reached BPM3 with a pulse width of a few tens of microseconds. A dc extraction test was also performed and two-dimensional (2D) images of the ions on BPM3 were observed. In the dc extraction mode, the length of extraction was successfully controlled from a few tens of seconds to 100 s. Figure 6(b) shows an example of the 2D image of a 250 eV beam consisting of a mixture of  $H_3^+$ ,  $H_2^+$ , and protons observed with BPM3 when all the electrodes were biased according to the results of the simulation. Figures 6(a)

TABLE II. Transversal spread of the 250 eV beam at the final focal point of the beam line obtained from simulation (antiprotons) and from experiment (positive ions) at different potentials applied to the electrode F2. In the experimental cases, the background has been subtracted (10% of maximum count) from the data. For the simulated values, the same initial parameters were used as for the values presented in Table I.

F2 potential (V)	Simulation $x_{rms}=y_{rms}$ (mm)	Experimental $x_{rms}$ (mm)	Experimental $y_{rms}$ (mm)
1300	2.2	1.3	1.6
1500	1.1	1.2	1.1
1900	2.5	2.5	2.6

and 6(c) show images of a similar 250 eV beam but with under- and overfocused conditions obtained by applying too low or too high potential on electrode F2. It is seen that the calculated potential configuration gives the best result and also that the spot size is rather insensitive to a small variation of  $V_{33}$ , which is consistent with the values obtained from simulations shown in Table II. The number of ions detected with the dc mode extraction was comparable to that observed with the pulse mode extraction, i.e., the transmission efficiency does not depend very much on the extraction mode. Similar numbers of transmitted ions were also obtained for beam energies as low as 10 eV, however, the spot size increased slightly as the beam energy decreased, which is again consistent with the simulations previously described (see Table I). When positively charged ions were detected, the front surface of the MCP was biased at approximately  $-2$  kV. In order not to disturb the trajectory of the ions, a mesh at the ground potential is placed a few millimeters in front of the MCP, which however resulted in small dotted structures due to a local focusing effect. In the case of antiproton detection, the bias applied to the front surface of the MCP was only a few hundreds of volts, i.e., the image of the antiproton distribution was not deformed.

## B. Antiprotons

We have succeeded to store and cool more than  $10^6$  antiprotons per AD shot.<sup>11</sup> From the annihilation rate during trapping, the background pressure in the trap was estimated to be roughly  $1 \times 10^{-13}$  Torr. The cooled antiprotons were then extracted toward the experimental chamber through the beam line. In order to monitor the annihilation position of the extracted antiprotons, two sets of track detectors were prepared, one of which was set several tens of cm apart in parallel to the magnet and the other positioned close to the beam line. Each track detector consisted of two 2 m long plastic scintillator bars, which are configured so that the magnetic field axis and the two scintillator bars were all in the same plane. When an energetic charged particle hits the bar, scintillation photons are emitted which are detected by photomultipliers attached on both ends of the bar. The hit position is derived from the arrival time difference between the two photomultipliers. When the energy of a  $p$  ion produced during antiproton annihilation is high enough, it can penetrate through the two scintillator bars. In this case, the annihilation position can be traced back with the two hit positions.

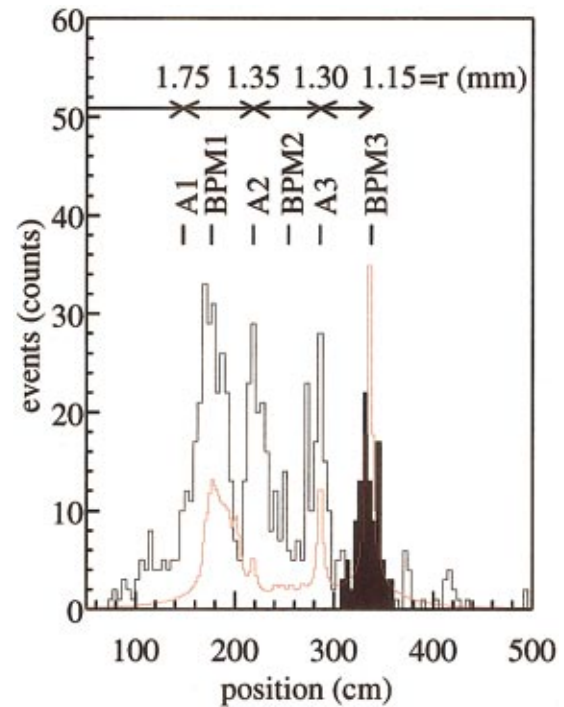


FIG. 7. (Color) In black: An example of the annihilation distribution measured with the beam line track detector for 250 eV antiprotons. Calculated annihilation positions in the beam line vs initial radial position in the trap are indicated in the upper part of the panel. In red: A simulated annihilation distribution.

The black histogram in Fig. 7 shows an example of the measured annihilation position distribution along the extraction beam line for an antiproton beam extracted at 250 eV and with the magnetic field at 2.5 T in the MRT. Extractions at 100 eV and 10 eV were also tried giving similar distributions and number of events. As can be observed, the distribution exhibits several peaks along the extraction beam line. The peaks corresponding to apertures A2 and A3 of lenses L2 and L3, respectively, are clearly identifiable while the limited effective detection area of the detector explains the absence of a peak corresponding to the aperture A1 of lens L1. Annihilations were also observed between apertures A1 and A2. The peak at 340 cm corresponds to annihilation at BPM3. To analyze the aforementioned annihilation distribution, antiproton trajectories were again simulated as a function of the initial radial position  $r$  of the antiproton in the trap, which are then compared with the inner radii of the electrodes (35 mm) and the aperture size (in this case with radii 3 mm). Considering that an antiproton annihilates whenever it touches material, the expected annihilation positions are indicated as a function of the initial radial position in the upper part of Fig. 7. It is seen that antiprotons annihilate (1) upstream of A1 or at A1 for  $r > 1.75$  mm, (2) between A1 and A2 for  $1.75 \text{ mm} > r > 1.35$  mm, (3) at A2 for  $r \approx 1.35$  mm, (4) between A2 and A3 for  $1.35 \text{ mm} > r > 1.30$  mm, and at A3 for  $1.30 \text{ mm} > r > 1.15$  mm. We can thus determine that at least a part of the antiproton cloud in the MRT during the experiments was within a radius of 1.7 mm from the center axis. The red histogram shows a simulated annihilation position distribution assuming a trapped antiproton cloud of radius 1.7 mm, homogenous density, and

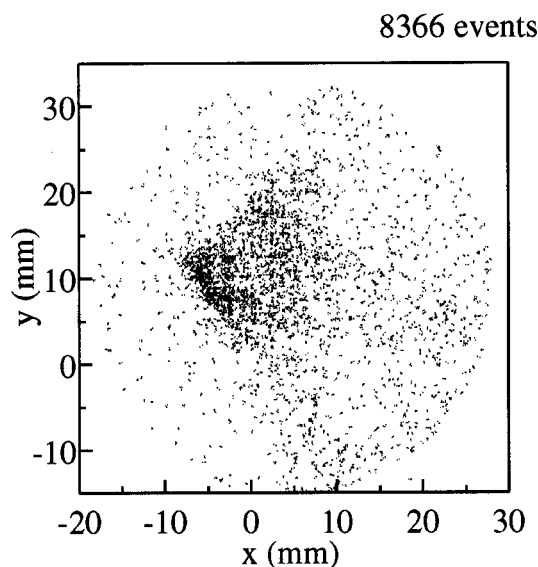


FIG. 8. The dot plot of particles reaching the delay line anode MCP detector at the focal point of the extraction beam line during 250 eV antiproton extraction.

cylindrical shape. Furthermore, the antiprotons leave the trap region with no transversal momentum. Both the spatial efficiency and the resolution of the detector were taken into account in the creation of this distribution. It can be observed that an overall annihilation pattern is more or less reproduced except that the resulting relative intensity between the peaks observed in the simulated distribution is quite different from the relative intensity between the peaks found in the experimentally acquired distribution. It is thus clear that during these initial tests, the extraction conditions were not yet optimized.

An image of particles reaching BPM3 during antiproton extraction is shown in Fig. 8. The number of observed events per shot was around  $10^3$ , which was comparable to those assigned as annihilations at BPM3 as observed by the track detector (see the black area indicated in Fig. 7) taking into account its solid angle and the multiplicity of the charged  $p$  ions emitted from each event. It is seen that the spot size was a couple of times larger than that observed for extracted positive ions. Considering that (1) the magnetic field for the former case was 2.5 times stronger than that of the latter

case, and (2) the mass ratio between antiprotons:  $H_2^+ : H_3^+$  is approximately 1:2:3, the observed spot size difference seems somewhat reasonable. Furthermore, a radial outward separation of antiprotons from electrons may take place,<sup>15</sup> which increases the radius of the antiproton cloud, decreases the transmission efficiency, and results in a larger focal point size.

Future extraction experiments will show if an improvement of the beam quality and a higher transmission efficiency can be obtained by compression of the antiproton cloud, which was successfully made for electrons<sup>16</sup> and ions<sup>11</sup> utilizing the same system. The system is now ready for further optimization at CERN.

#### ACKNOWLEDGMENTS

The authors are most grateful to the AD and RFQD staff at CERN for providing the antiproton beam. Postdoctoral Fellowships from the Japanese Society for the Promotion of Science (JSPS) and the Science and Technology Agency (STA) financially supported four of the authors (K. Y. F., H. H., M. H., and Z. W.) during these experiments. The work is supported by the Grant-in-Aid for Creative Basic Science (Grant No. 10P0101), Japanese Ministry of Education, Science, and Culture, and by the Hungarian Science Foundation (OTKA T033079 and TeT JAP-00/04).

<sup>1</sup>ASACUSA collaboration proposal, CERN/SPSC 97-19, SPSC P-307 (1997).

<sup>2</sup>J. Bosser *et al.*, CERN PS/HP Note-97-36 (1997).

<sup>3</sup>A. M. Lombardi *et al.*, Proceedings of the 2001 Particle Accelerator Conference, Chicago, IL, 2001, p. 585.

<sup>4</sup>Y. Yamazaki, Nucl. Instrum. Methods Phys. Res. B **154**, 174 (1999).

<sup>5</sup>Y. Yamazaki, AIP Conf. Proc. **498**, 48 (1999).

<sup>6</sup>T. Ichioka, H. Higaki, M. Hori, N. Oshima, K. Kuroki, A. Mohri, K. Komaki, and Y. Yamazaki, AIP Conf. Proc. **498**, 59 (1999).

<sup>7</sup>K. Yoshiki Franzen *et al.*, AIP Conf. Proc. **606**, 79 (2002).

<sup>8</sup>A. Mohri *et al.*, Jpn. J. Appl. Phys., Part 1 **37**, 664 (1998).

<sup>9</sup>L. S. Brown and G. Gabrielse, Rev. Mod. Phys. **58**, 233 (1986).

<sup>10</sup>H. Higaki, N. Kuroda, T. Ichioka, K. Yoshiki Franzen, Z. Wang, K. Komaki, Y. Yamazaki, M. Hori, N. Oshima, and A. Mohri, Phys. Rev. E **65**, 046410 (2002).

<sup>11</sup>N. Kuroda *et al.* (unpublished).

<sup>12</sup>M. Reiser, *Theory and Design of Charged Particle Beams* (Wiley, New York, 1994), p. 59.

<sup>13</sup>R. E. Marrs, Nucl. Instrum. Methods Phys. Res. B **149**, 182 (1999).

<sup>14</sup>M. Hori (unpublished).

<sup>15</sup>T. M. O'Neil, Phys. Fluids **24**, 1447 (1981).

<sup>16</sup>T. Ichioka, Ph.D. thesis, University of Tokyo, 2001.